METHODS FOR DETERMINING FUNDAMENTAL CHEMICAL DIFFERENCES BETWEEN IRON DISULFIDES FROM DIFFERENT GEOLOGIC PROVENANCES[1]

Richard W. Hammack,[2] Ralph W. Lai,[3] and J. Rodney Diehl[3]

Abstract.--X-ray photoelectron spectroscopy (XPS), evolved gas analysis (EGA), and froth flotation tests were used to compare iron disulfides of hydrothermal, sedimentary/hydrothermal, and sedimentary origin. A specimen composed of equal amounts of pyrite and marcasite was also evaluated. The susceptability of iron disulfide surfaces to oxidation was measured using XPS and EGA techniques. XPS analyses indicated the following order of increasing oxidation rate at 21 pct oxygen and 88 pct relative humidity: sedimentary/hydrothermal pyrite (0.70 mg SO_4^{-2}/hr per gram of FeS_2)< hydrothermal pyrite (0.83 mg SO_4^{-2}/hr per gram of FeS_2)< hydrothermal pyrite/marcasite (1.34 mg SO_{4-2}/hr per gram of FeS_2)< sedimentary pyrite (3.53 mg SO_4^{-2}/hr per gram of FeS_2). Oxidation rates measured by XPS are based solely on the sulfate/sulfide ratios at the surface, where oxidation is not inhibited by mass transfer limitations. Therefore, these rates are much higher than previously published rates based on bulk iron disulfide content. The comparison of EGA results with oxidation rates measured by XPS showed that for sedimentary pyrites, higher temperatures of SO_2 evolution corresponded to lower oxidation rates. Weathering rates for hydrothermal iron disulfides appear to be independent of SO_2 evolution temperatures. In flotation tests with an anionic fluorosurfactant collector, hydrothermal pyrite floated and sedimentary pyrite was depressed. Hydrothermal pyrite floated because it developed a positive surface charge in solution that allowed the attachment of the anionic collector. The negative charge developed by sedimentary pyrite in this solution repelled the anionic collector, depressing sedimentary pyrite. This research provides a better understanding of iron disulfide oxidation and illustrates inherent differences in physical and chemical properties that significantly alter the behavior of pyrites of different geologic provenance.

[1]Paper presented at the 1988 Mine Drainage and Surface Mine Reclamation Conference sponsored by the American Society for Surface Mining and Reclamation and the U.S. Department of the Interior (Bureau of Mines and Office of Surface Mining Reclamation and Enforcement), April 17-22, 1988, Pittsburgh, PA.

[2]Richard W. Hammack is a Geologist, Pittsburgh Research Center, U.S. Department of the Interior, Bureau of Mines, Pittsburgh, PA.

[3]Ralph W. Lai is a Metallurgist, and J. Rodney Diehl is a Physical Scientist, U.S. Department of Energy, Pittsburgh Energy Technology Center, P.O. Box 10940, Pittsburgh, PA.

Proceedings America Society of Mining and Reclamation, 1987 pp 136-146
DOI: 10.21000/JASMR88010136

INTRODUCTION

The weathering of sulfide minerals accounts for most of the surface water and groundwater contamination that results from mining. Pyrite, the most prevalent sulfide mineral, is primarily responsible for the acid discharges from underground coal and metal mines, surface mine spoils, and tailings (refuse) disposal areas. In general, not all pyrites weather at the same rate. This fact is apparent to anyone who has compared unweathered pyrite from a 50-year-old metal mine dump with pyrite from coal refuse that becomes encrusted with hydrated iron sulfates and oxyhydroxides (pyrite weathering products) in a matter of days. The rate at which pyrites oxidize varies significantly with surface area; many authors (Pugh and others, 1981; Pugh and others, 1984; and Nicholson and others, 1987) have shown that there is a positive, linear correlation between surface area and the rate of pyrite oxidation. Pyrites of sedimentary (low-temperature) origin typically display greater surface area, due to smaller mean particle size and greater surface irregularity, than pyrites of hydrothermal (high-temperature) origin. Therefore, sedimentary pyrite would be expected to be more reactive than hydrothermal pyrite. However, recent work (Esposito and others, 1987) has suggested that differences in surface area do not adequately explain differences in pyrite solubility.

In this study, pyrites of three different origins (sedimentary, sedimentary/hydrothermal, and hydrothermal) were compared, using x-ray photoelectron spectroscopy (XPS) weathering tests, evolved gas analysis (EGA), and flotation response measurements. A hydrothermal specimen containing about equal amounts of pyrite and marcasite was also evaluated. The intent of this study was to determine if surface area differences are solely responsible for the wide range of observed pyrite reactivities, or if fundamental chemical differences must also be considered. We also wished to determine if a simple analytical technique, such as EGA, could be used to quickly predict the rate at which different pyrites oxidize.

TECHNICAL APPROACH

XPS Weathering Tests

The intention was to measure only oxidation on the surface of iron disulfide particles where mass transfer effects are minimized. By minimizing mass transfer or diffusional effects, we hoped to measure rates that more accurately reflect the chemical kinetics of iron disulfide oxidation. Because rates measured in this study are based on the amount of iron disulfide at the surface and "available" for reaction, these rates are significantly faster (10 to 20 times) than rates typically reported for iron disulfide oxidation. Previous studies have based observed oxidation rates on bulk pyrite content (amount of sulfate produced or oxygen consumed per gram of bulk pyrite per hour), although only a small fraction of the bulk pyrite was at the surface and available for reaction. Available pyrite can be calculated from the bulk pyrite content, using surface area estimation or gas absorption techniques, but this calculation involves several approximations and can only be regarded as an estimate.

In contrast to previous studies, a surface analysis technique (XPS) that detects both pyritic sulfur and sulfate sulfur at the point of reaction was used. XPS provides quantitative elemental information with a detection limit of approximately 1 pct of atoms comprising the outermost monolayer. Different formal oxidation states can be distinguished, based on chemical shift information. Chemical shifts in the sulfur (2p) electron binding energy (fig. 1) were used in this study to distinguish between pyritic sulfur (reactant) and sulfate sulfur (product). The XPS analysis depth for pyrite is estimated to be about 2.3 nm, based on measured inelastic mean free paths for similar semiconductors (Buckley and others, 1987). This depth corresponds to the thickness of 4.24 pyrite unit cells (0.54175 nm/unit cell).

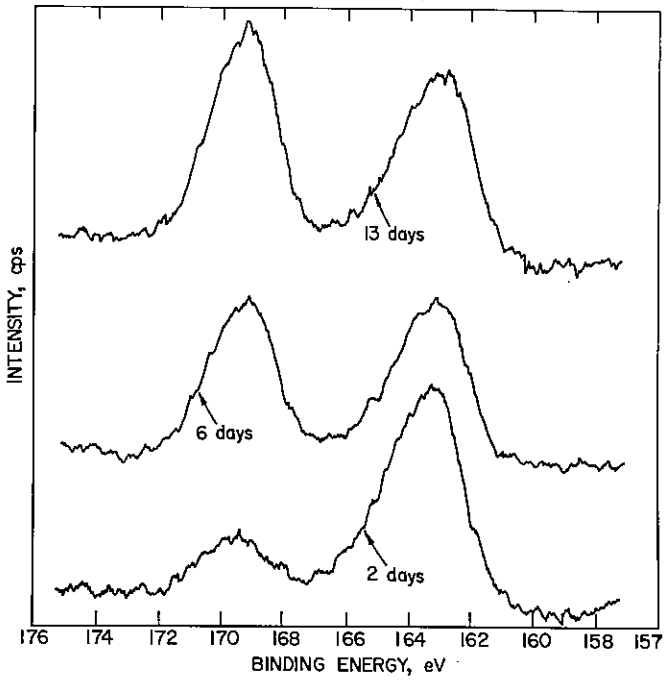

Figure 1. XPS SCAN of the sulfur (2p) region showing pyritic sulfur (B.E. = 163.5eV) and sulfate sulfur (B.E. =169.5eV) after 2, 6, and 13 days weathering.

Most published studies (Braley, 1960; Clark, 1965; Rogowski and Pionke, 1984; and Nicholson and others, 1987) have used sulfate production as a measure of the amount of oxidation that has taken place. In these studies, sulfate cannot be detected until it is dissolved and leached from the sample. This adds the complexity of sulfate solubility, pH-dependent sulfate adsorption, and sulfate transport considerations. Oxidation rates based on insitu detection of "available" pyrite and sulfate are better than rates based on "bulk" pyrite and leached sulfate for determining the mechanism and kinetics of pyrite oxidation. Because oxidation products were not leached from pyrite surfaces, the XPS technique permitted us to monitor, for the first time, the response of the oxidation rate to the accumulation of oxidation products.

Iron disulfides were weathered at a constant humidity of 88, pct but at different oxygen partial pressures. The conversion of sulfide sulfur to

sulfate sulfur was monitored. For each sample, a percent conversion was calculated from the integrated photoelectron intensities for sulfate sulfur (binding energy = 169 eV) and pyritic sulfur (binding energy = 163 eV):

$$\text{Percent conv.} = \frac{I \text{ sulfate sulfur}}{(I \text{ sulfate sulfur} + I \text{ sulfide sulfur})} \times 100 \text{ pct.}$$

where I = integrated photoelectron intensity.

Because sulfate sulfur and sulfide sulfur were the only observed sulfur species, the equation can be rewritten.

$$\text{Percent conv.} = \frac{I \text{ sulfate sulfur}}{I \text{ total sulfur}} \times 100 \text{ pct}$$

Evolved Gas Analysis

Evolved gas analysis is a thermal analysis technique that employs a programmable tube furnace to heat samples in an oxidizing atmosphere. The concentrations of gases evolved from the sample are monitored with respect to sample temperature. This study monitored the sulfur dioxide evolved from the high-temperature, anhydrous oxidation of iron disulfides:

$$2\ FeS_2 + 5.5\ O_2 \rightarrow Fe_2O_3 + 4\ SO_2$$

Reactive iron disulfides are expected to oxidize and evolve sulfur dioxide at lower temperatures (lower activation energy) than more stable forms. Therefore, the sulfur dioxide evolution temperature can serve as a qualitative indicator of oxidation rate. EGA can rank iron disulfides in order of increasing reactivity by the anhydrous oxidation pathway but the correlation of sulfur dioxide evolution temperatures to hydrous, room temperature oxidation rates had not been established prior to this study.

SAMPLE DESCRIPTION

Pyrites from three different origins were tested in this study: a hydrothermal pyrite from Rico, Colorado; a pyrite of sedimentary origin that was later metamorphosed (sedimentary/hydrothermal pyrite) from the Mammoth anthracite seam in eastern Pennsylvania; and a sedimentary pyrite from the Upper Freeport coalbed, Coshocton County, Ohio. The hydrothermal pyrite/marcasite was from Joplin, Missouri. Additional iron disulfide samples that were not subjected to all tests included: sedimentary pyrites from the Pittsburgh coalbed, Barbour County, West Virginia (one sample) and from carbonaceous shales overlying the Clarion coalbed, Clearfield County, Pennsylvania (two samples); a hydrothermal pyrite from the Noranda Mine, Quebec, Canada; and a hydrothermal marcasite from Joplin, Missouri. Each sample for XPS and EGA analysis was crushed to a -150 to +200-mesh size fraction and centrifuged in acetyl tetrabromide (2.96 specific gravity) at 1500 rpm for 20 minutes to separate the iron disulfide from less dense clays, coal, and accessory minerals. The sink fraction was then washed with certigrav (1.20 specific gravity) to remove residual bromine. X-ray diffraction of the cleaned iron disulfides indicated that some mineral contaminants remained. These contaminants are listed in Table 1.

TEST PROCEDURES

XPS Weathering Tests

Immediately prior to weathering, samples for XPS analysis were washed with boiling 4.8 N HCl to remove sulfate, rinsed with methanol, and dried under vacuum. For each sample, thirty cylindrical wafers (13 mm diameter by 0.5 mm) were pressed under 700 kg/cm^2 pressure. Ten wafers of each sample were weathered simultaneously under the same conditions. Atmospheres used for this study contained 5, 10, and 21 pct oxygen (balance, nitrogen) at 88 pct relative humidity. Weathering chambers (fig. 2) were constructed so that wafers could be removed without disturbing or contaminating the atmosphere within the chamber. A total of three chambers were used so that samples could be weathered under all three atmospheres, simultaneously. Prior to each experiment, the chambers were washed with an acidified surfactant (sodium lauryl sulfate) solution and then rinsed with methanol to reduce the likelihood of bacterial catalysis. Periodically during the test, one wafer from each rod was removed from the chamber and placed in a Leybold-Heraeus LHS-10 photoelectron spectrometer operated at a pressure of $2X10^{-8}$ mbar or lower. X-rays from a magnesium anode (MgKα = 1253.6 eV) and an analyzer pass energy of 100 eV were used for the acquisition of S(2p) and Fe(2p) spectra. Binding energy calibrations were carried out by adjusting the measured binding energy for the C(1s) spectrum of adventitious carbon to 284.6 eV and shifting all other measured binding energies correspondingly. Peak areas within the S(2p) region attributable to sulfide sulfur and sulfate sulfur were determined with the Leybold-Heraeus DS-5 data system. The percent conversion was calculated for each wafer and plotted versus weathering time.

Table 1.--Mineral contaminants in iron disulfide samples.

Iron Disulfide	Mineral Contaminant(s)
Hydrothermal pyrite	Calcite
Sedimentary/ hydrothermal pyrite	Kaolinite, calcite, quartz, and dolomite
Sedimentary pyrite	Kaolinite, quartz, calcite, and marcasite
Hydrothermal pyrite/ marcasite	Quartz

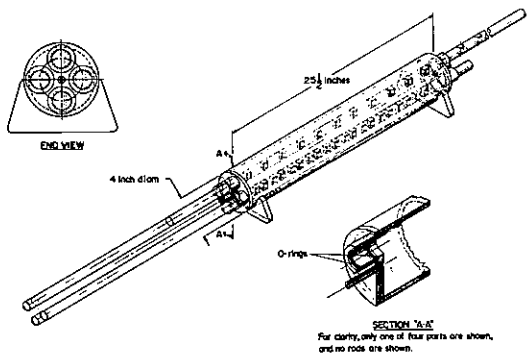

Figure 2. Schematic of weathering chamber used in this study.

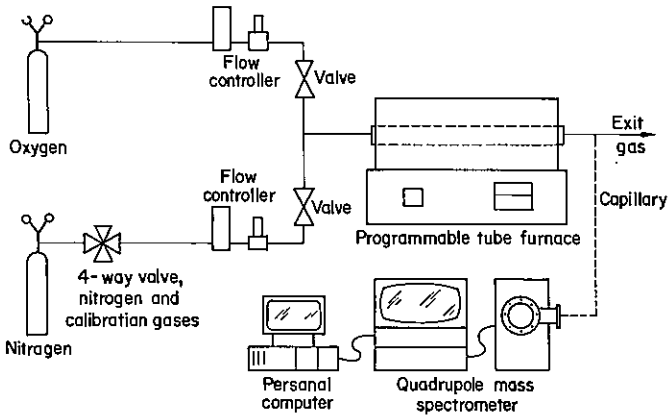

Figure 3. Schematic of evolved gas analysis instrument.

EGA Tests

An instrument designed specifically for evolved gas analysis was used. This instrument (fig. 3) is similar to an evolved gas instrument constructed by LaCount and others (1983). Major components include an electronic mass flow controller/gas blender, a programmable tube furnace, a quadrupole mass spectrometer, a programmable analog to digital (A/D) converter, and a microcomputer.

The electronic mass flow controller/gas blender can provide selectable flow rates from 0.1 to 200 mL/min. It can also provide two-component gas mixtures ranging from 0.1 to 99.9 percent. In this study, a 10.0 percent oxygen/90.0 percent nitrogen mixture was introduced into the tube furnace at a flow rate of 100 mL/min.

Fifty milligrams of sample was diluted with 3g of tungsten oxide to insure uniform heating. The sample was then placed in a 2.54 cm diameter by 50 cm long quartz tube and secured with either glass wool or quartz wool, depending upon the maximum test temperature. A 32 mm (1/8 in), Type K thermocouple was inserted into the sample and the tube then placed in the furnace. Output from the thermocouple was conditioned by a linearizer and then passed to an A/D converter.

The tube furnace used was capable of performing two heating ramps with selectable heating rates, dwell temperatures, and dwell times. Starting at about 70°C, the sample was heated at a rate of 6°C/min up to 380°C. The heating rate was then decreased to 3°C/min up to 720°C, where each run was terminated.

Evolved gases were detected with a quadrupole mass spectrometer. The capillary inlet to the spectrometer was placed immediately downstream from the sample to minimize lag time between gas evolution and detection. The mass spectrometer was capable of simultaneously monitoring the ion current at 12 user-selected mass to charge ratios (M/e), although only the ion current at the M/e ratio of sulfur dioxide (64) is of interest here. This ion current was converted to partial pressure by multiplying by the calibration factor for sulfur dioxide. The partial pressure of sulfur dioxide and sample temperature were transmitted to a microcomputer where the data were converted to ASCII files and written to floppy disk. Commercially available graphics, gaussian peak fitting, and integration software were used to manipulate data.

Table 2.--Surface oxidation rates of iron disulfides at 88 pct relative humidity and 5 pct, 10 pct, and 21 pct oxygen.

Sample	Oxidation Rate ($mg\ SO_4^{-2}\ g^{-1}\ FeS_2\ hr^{-1}$) 5 pct O_2	10 pct O_2	21 pct O_2
Sedimentary pyrite	1.85	N.D.[1]	3.54
Hydrothermal pyrite/ marcasite	0.92	1.03	1.33
Hydrothermal pyrite	0.78	0.88	0.83
Sedimentary/ hydrothermal pyrite	0.41	0.54	0.70

[1]Not Determined--insufficient number of samples.

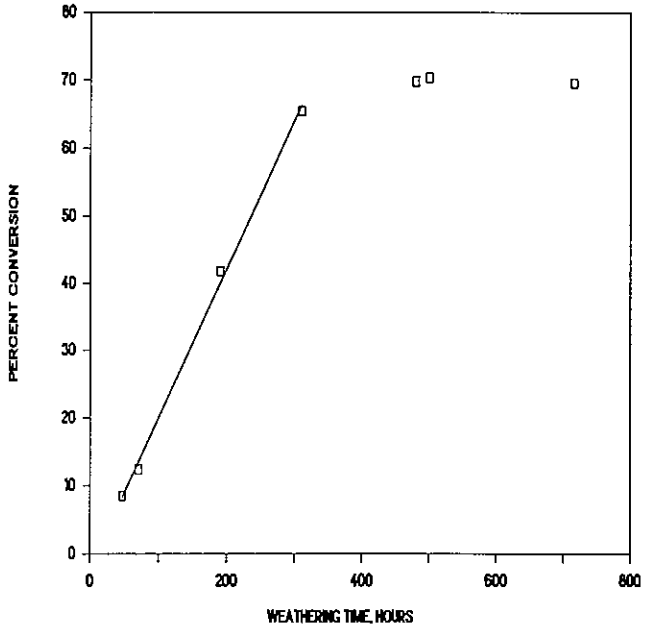

Figure 4. XPS monitored weathering of sedimentary pyrite at 21 pct. oxygen and 88 pct. relative humidity. Solid line denotes the least squares regression line used for rate calculations.

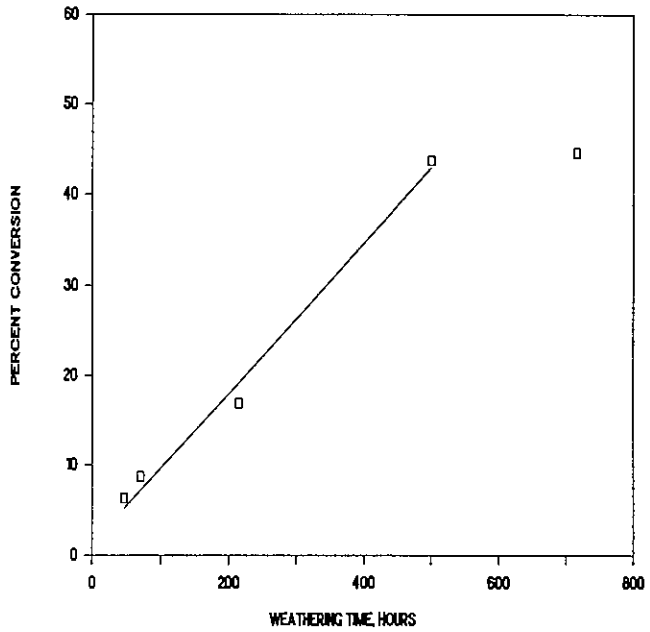

Figure 5. XPS monitored weathering of pyrite/ marcasite at 21 pct. oxygen and 88 pct. relative humidity. Solid line denotes the squares regression line used for rate calculations.

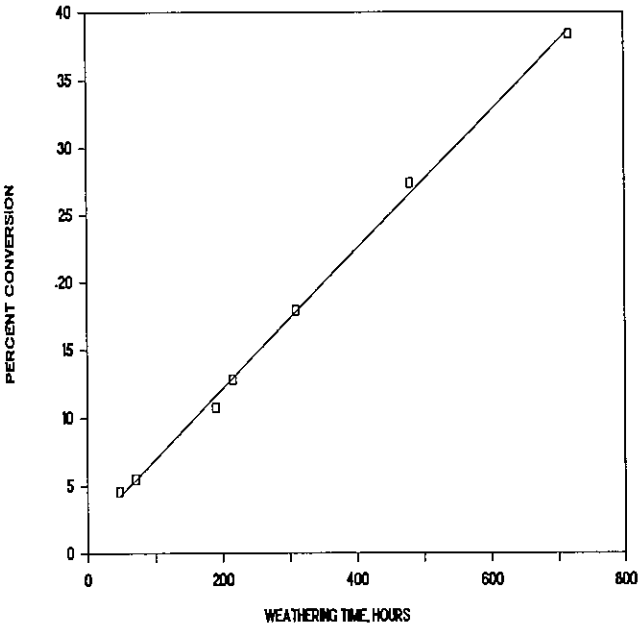

Figure 6. XPS monitored weathering of hydrothermal pyrite at 21 pct. oxygen and 88 pct. relative humidity. Solid line denotes the least squares regression line used for rate calculations.

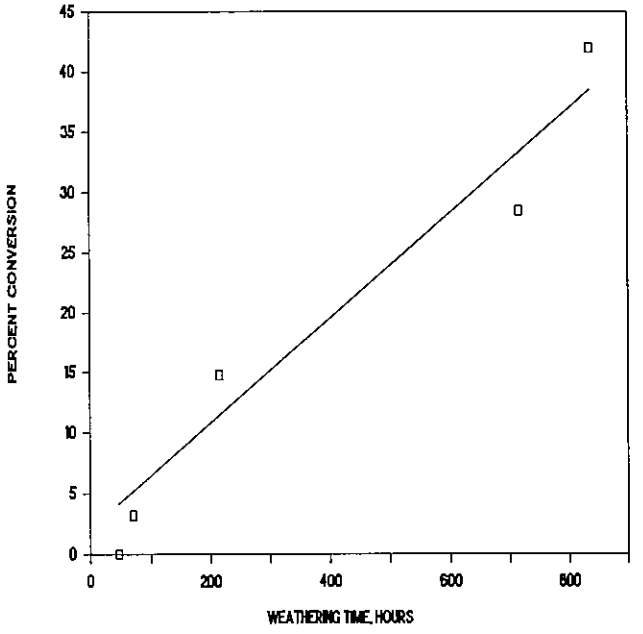

Figure 7. XPS monitored weathering of sedimentary/ hydrothermal pyrite (anthracite pyrite) at 21 pct. oxygen and 88 pct. relative humidity. Solid line denotes the least squares regression line used for rate calculations.

RESULTS AND DISCUSSION

XPS Tests

Plots of percent conversion of pyritic sulfur to sulfate sulfur versus weathering time (figs. 4-7) exhibited an initial linear region representing oxidation of about 40 to 90 percent of the available pyritic sulfur. Abiotic oxidation rates for each iron disulfide (table 2) were calculated from the slope of the least squares line fitted to the data in the initial linear region (solid line, figs. 4-7). Similar plots were obtained for tests at 5 pct and 10 pct oxygen.

The rates in table 2 reflect abiotic surface oxidation as measured by XPS. Because only pyritic sulfur and sulfate sulfur on the surface are detected, this technique can be used to compare the oxidation rates of iron disulfides with significantly different surface areas. Oxidation rates are simply the change in the sulfate sulfur:pyritic sulfur ratio with respect to time.

In samples with high surface area, more pyritic sulfur is detected by XPS, because more pyrite is exposed at the surface. Therefore, the technique compensates for differences in surface area and permits the oxidation of each iron disulfide to be monitored under near-ideal conditions. It is evident from the oxidation rates in table 2 that sedimentary pyrite is significantly more reactive than pyrite of high temperature (hydrothermal) origin irrespective of surface area. Sedimentary/hydrothermal pyrite, which originally formed at low temperatures (< 50°C) and was later metamorphosed, displayed a reactivity similar to hydrothermal pyrite. Even the specimen containing roughly equal parts hydrothermal pyrite and hydrothermal marcasite exhibited a reactivity that was closer to hydrothermal pyrite than to sedimentary pyrite.

The dependence of the abiotic oxidation of iron disulfides (initial rates) on oxygen content is shown in figure 8. Oxygen dependency ranges from no apparent dependence (0th order) in the case of hydrothermal pyrite to a significant dependence in the case of sedimentary pyrite. Both pyrite/marcasite and sedimentary/hydrothermal pyrite exhibited a similar but slight oxygen dependency. The number of oxygen partial pressures tested in this study is insufficient for formulating rate equations or determining reaction order. However, the difference in oxygen dependence between pyrites of pure sedimentary origin and pyrites of predominantly hydrothermal origin appears to be significant.

Sedimentary pyrite and pyrite/marcasite specimens reached an asymptotic level within the 800-hour experiments (70 pct. conversion, fig. 4 and 45 pct. conversion, fig. 5) where no further oxidation took place. The presence of an asymptote indicates that the mineral surface has become passivated. Possible explanations for this apparent passivation include the following:

1. The exhaustion of pyrite on the surface (applicable if XPS is detecting pyrite below the depth of weathering);

2. The exhaustion of a more reactive pyrite form (remaining pyrite oxidizes at a slow rate that is undetectable within the time frame of these tests);

3. In the case of sedimentary pyrite, organic sulfur in the form of thiophenes, thiols and organic sulfides would appear at the same binding energy as pyrite but would be unreactive;

4. A metal-deficient sulfide layer forms that cannot be distinguished from pyritic sulfur, but is unreactive and passivates pyrite surfaces.

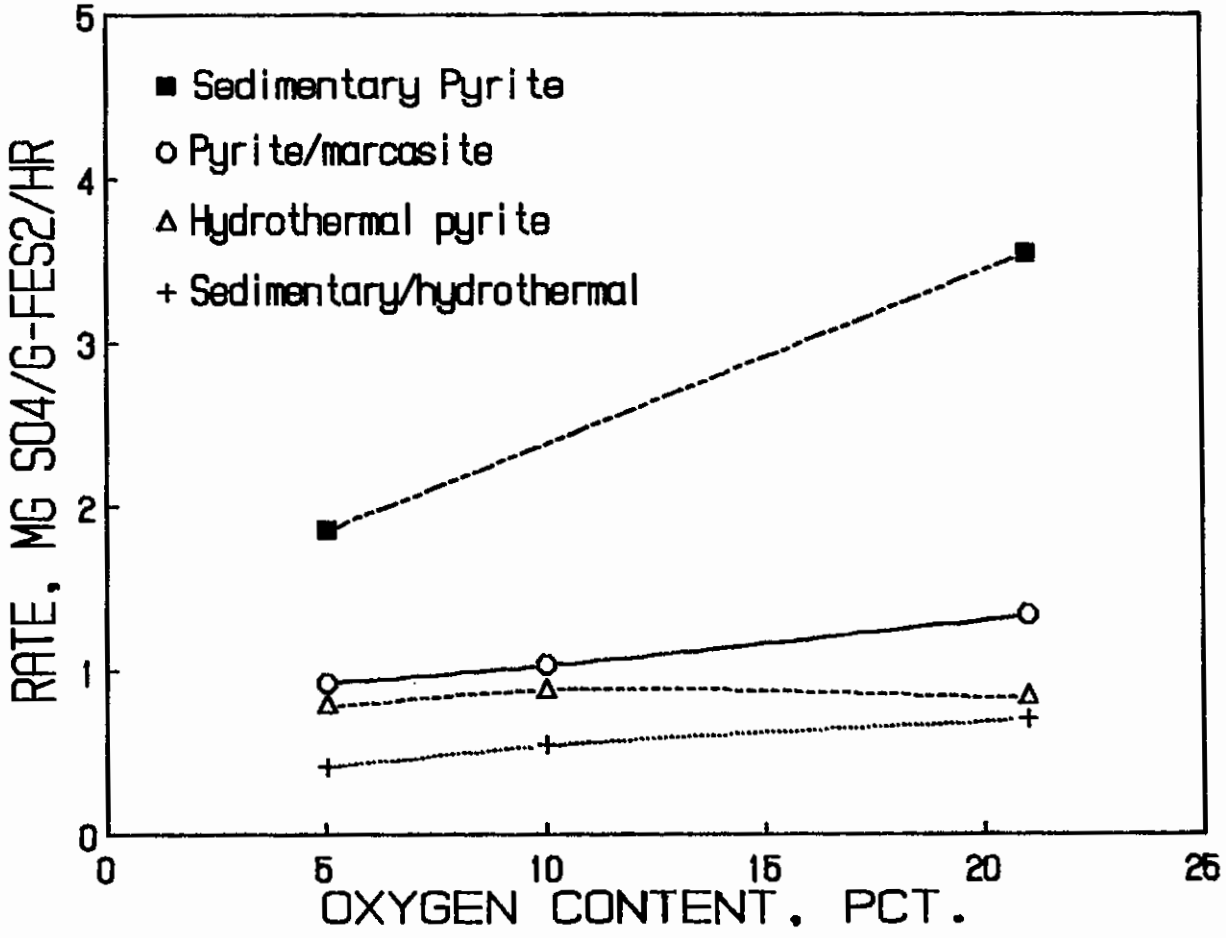

Figure 8. The dependence of oxidation rate on oxygen content.

Explanation 1 probably is not valid because we have observed in depth profiles (XPS analysis with argon ion sputtering), weathering 10-20 nm below the surface of sedimentary pyrite which is at least four times the analysis depth for XPS. Explanation 2 cannot be proved or disproved with current information. Explanation 3 may explain the presence of asymptotes in sedimentary pyrite plots, but not in hydrothermal pyrite/marcasite plots where no organic sulfur is present. Passivation due to the formation of a metal-deficient sulfide layer or the accumulation of oxidation products on the surface may best explain the asymptotes. Buckley and Woods (1986) found that upon weathering, a metal-deficient sulfide layer formed on pyrite which effectively passivated oxidation even in the presence of acetic acid. The S(2p) binding energy for this metal-deficient sulfide was 1- to 1.3-eV higher than that of pyrite and 0.3 eV lower than bulk elemental sulfur. In the work by Buckley and Woods, the metal-deficient sulfide only formed a small shoulder on the pyritic S(2p) peak (7 pct of the total S(2p) intensity). The resolution and the signal-to-noise ratio of the XPS instrument used in the present study were inadequate for the detection of metal-deficient sulfide layers.

EGA Tests

Plots of SO_2 partial pressure versus sample temperature are shown in figure 9. The mean temperature of the major peak for each iron disulfide increased in the following order: pyrite/marcasite (420°C), sedimentary pyrite (428°C), sedimentary/hydrothermal pyrite (470°C), and hydrothermal pyrite (499°C). When surface oxidation rate (21 pct oxygen, 88 pct relative humidity) measured by XPS is plotted versus the mean temperature of the major SO_2 evolution peak (fig. 10), two linear trends are observed. One trend, represented by five sedimentary pyrites, occurs at temperatures below 460°C with a slope of -0.103 mg SO_4 g^{-1} FeS_2 hr^{-1}/°C (r^2 = 0.9914). The second trend is represented by three pyrites of predominantly hydrothermal origin and exhibits a slope of -0.007 mg SO_4 g^{-1} FeS_2 hr^{-1}/°C (r^2 = 0.8293). A line connecting the two marcasite-containing samples parallels the slope of the sedimentary pyrite regression line, although it occurs at 30oC lower temperature. Based on the limited data available, sedimentary and hydrothermal pyrite appear to represent discrete populations that overlap at a SO_2 evolution temperature of 460°C. The linearity of the plot indicates that sedimentary pyrite specimens which are more susceptible to the high temperature, anhydrous oxidation in EGA, are also more susceptible to the hydrous oxidation in XPS tests that simulate the mine environment. However, the weathering rates for hydrothermal pyrite are low, irrespective of the major SO_2 evolution temperature displayed by the specimen.

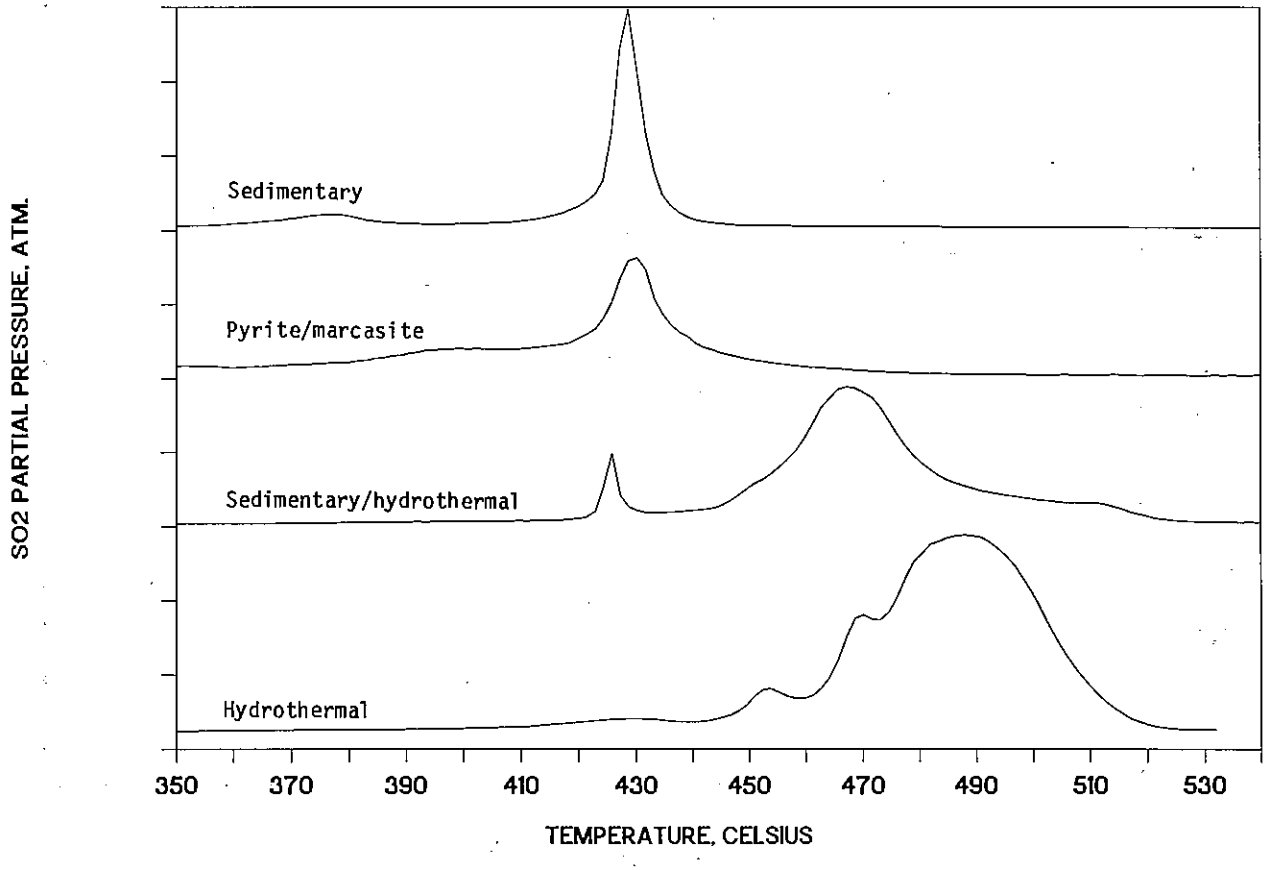

Figure 9. SO_2 thermograms of sedimentary pyrite, hydrothermal pyrite/marcasite, hydrothermal pyrite, and sedimentary/hydrdothermal pyrite.

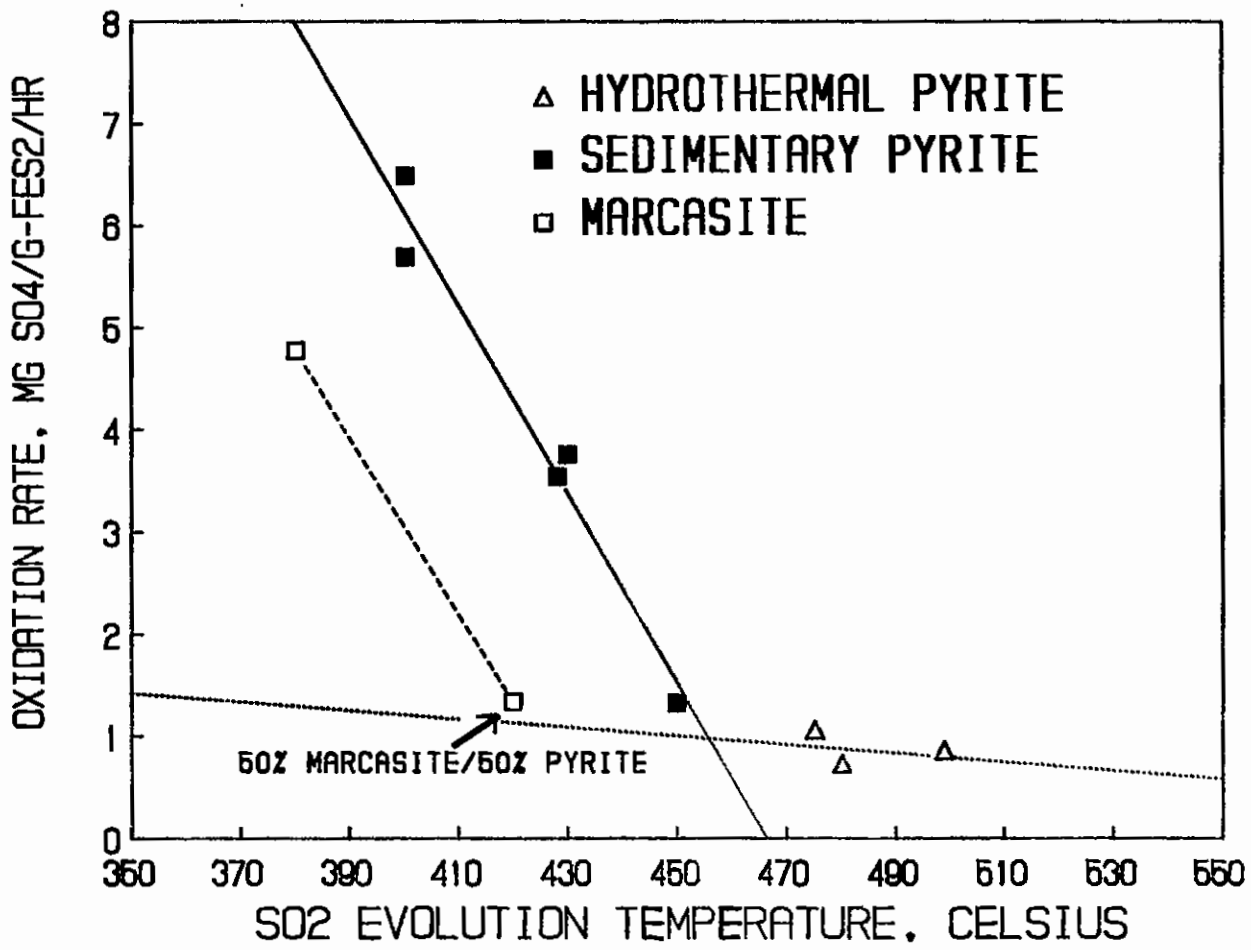

Figure 10. Plot of SO_2 evolution temperature from evolved gas analysis versus XPS monitored weathering rates.

The relationship between SO_2 evolution temperature and surface oxidation for sedimentary pyrites may permit EGA to be used as a quick method for determining surface oxidation rate. The sum of SO_2 peak areas was plotted versus mean evolution temperature for 16 coal samples from the Waynesburg, Upper Freeport, and Lower Kittanning coalbeds (fig. 11) and for 55 overburden samples from Pennsylvania, West Virginia, Maryland, Kentucky, and Illinois (fig. 12). The sum of the SO_2 peak areas is proportional to the total amount of pyrite with mean evolution temperatures within the 10°C interval. In both coal and overburden samples, most of the SO_2 is evolved from pyrite in the 420°C and 430°C intervals, which suggests that the abiotic surface oxidation rate is between 2.5- and 4.5 mg SO_4^{-2} g^{-1} FeS_2 hr^{-1}. Sulfur dioxide evolved at temperatures above 460°C is indicative of organic sulfur present in coal and other carbonaceous material (hydrothermal pyrite would also evolve SO_2 in this range if present). When the overburden samples (fig. 12) are compared with the coal samples (fig. 11), the distribution of the SO_2 peak areas appears to be 10°C higher in the case of the coal samples. This shift probably does not reflect a fundamental difference in pyrite reactivity, but rather a difference in sample preparation. The coal samples were crushed many months prior to EGA analysis, whereas the overburden samples were prepared and run within minutes. We have observed that with time and exposure to air, the SO_2 evolution temperature

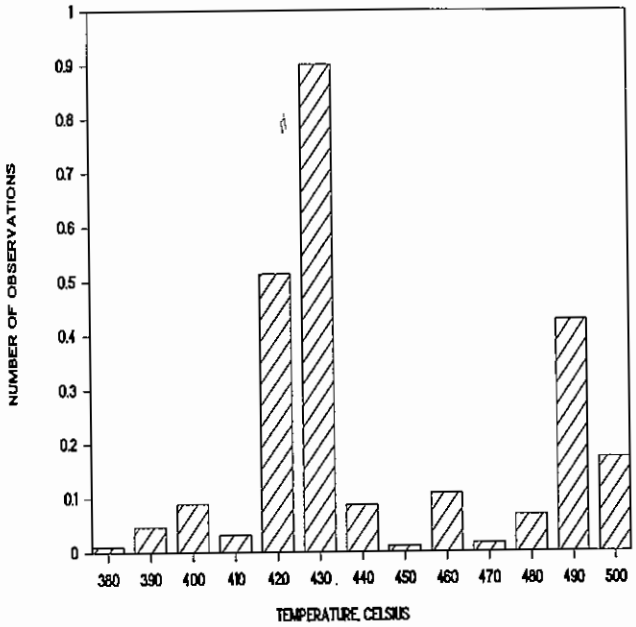

Figure 11. Distribution of SO_2 evolution temperatures for pyrite (≤460°C) and organic sulfur (>460°C) in 25 coal samples.

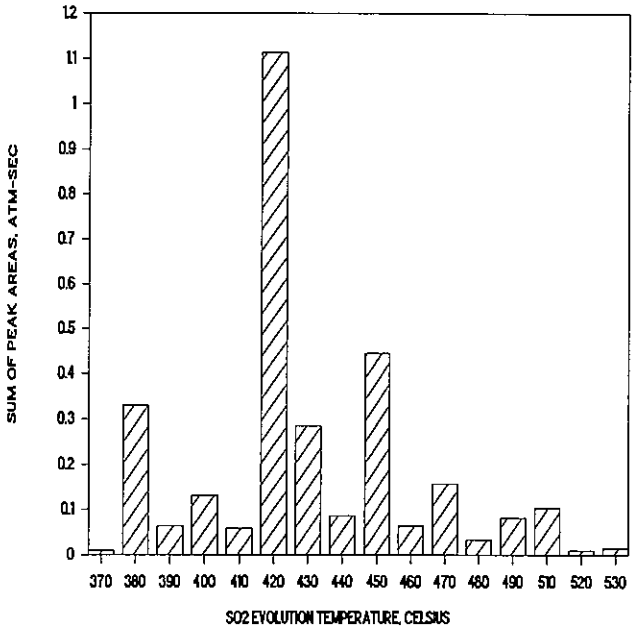

Figure 12. Distribution of SO_2 evolution temperatures for pyrite and organic sulfur in 55 over-burden samples.

increases. Another feature of these distributions is the small peak in the range of 380°C to 400°C that corresponds to the low temperature peak in the SO_2 thermogram of sedimentary pyrite (figs. 9 and 13). Pure marcasite also evolves SO_2 in this range (fig. 13) and it is possible that the small peak commonly observed in the SO_2 thermograms of sedimentary samples may represent marcasite. A small peak at 450°C (fig. 12) probably indicates that a more stable, epigenetic form of sedimentary pyrite is sometimes present.

Flotation Tests

XPS and EGA results indicate that sedimentary and hydrothermal iron disulfide surfaces exhibit significantly different reactivity. To help explain these differences, we used a simple froth flotation test to determine the charge developed on pyrite surfaces in aqueous solutions. This test consisted of placing a two-gram sample of -100 mesh pyrite in a 100-mL Pyrex glass flotation cell with a fritted bottom for gas bubbling. Each sample was conditioned in a solution containing 300 ppm anionic fluorosurfactant and 5 ppm sodium hydrosulfide, and then subjected to a three minute flotation. The froth and the residue were collected, dried, weighed, and the percentage flotation calculated. The flotation response of a sedimentary and a hydrothermal pyrite is given in Table 3.

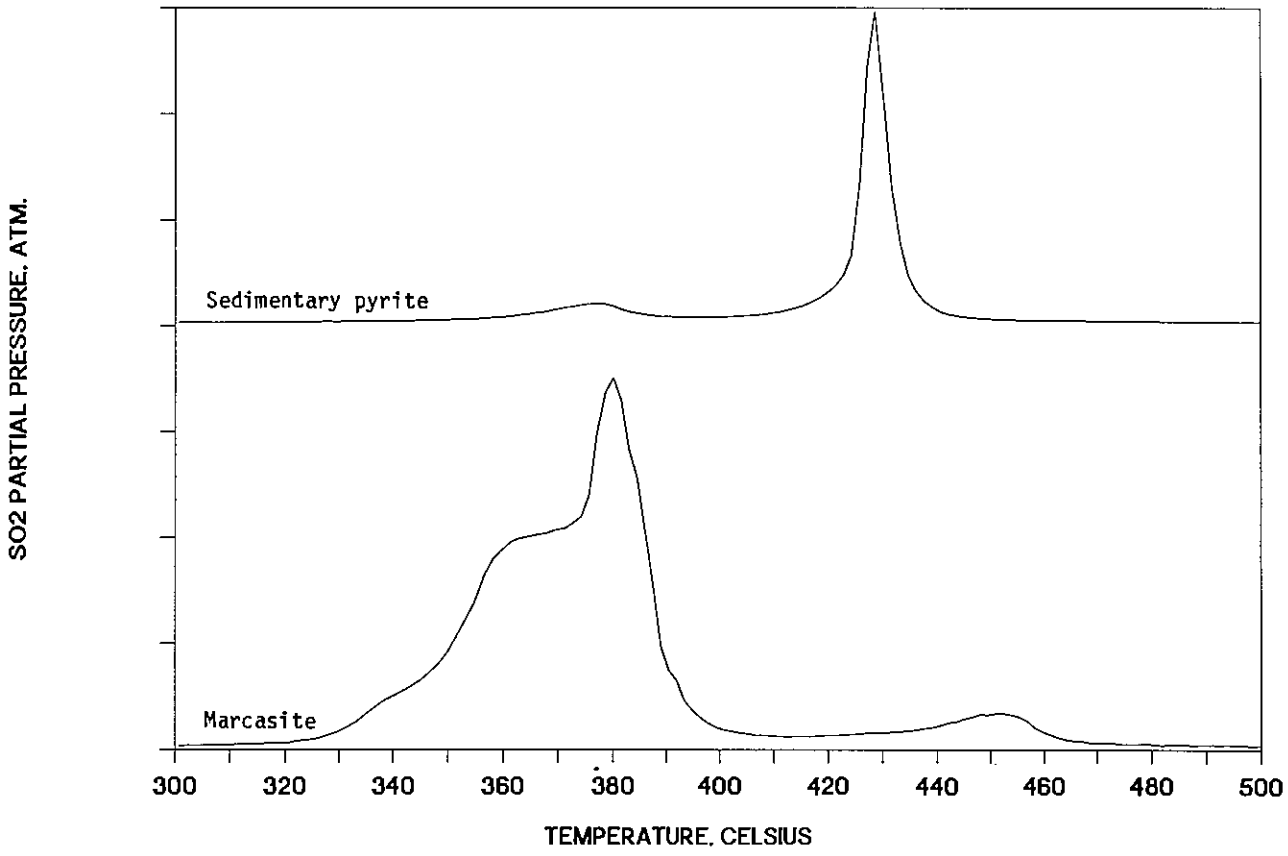

Figure 13. SO_2 thermograms of hydrothermal marcasite and sedimentary pyrite.

Table 3.--Flotation response of hydrothermal and sedimentary pyrites.

Sample	Wt. % Floated	Surface Charge
Hydrothermal pyrite	32	Positive
Sedimentary pyrite	<1	Negative

Hydrothermal pyrite and sedimentary pyrite differed substantially in flotation response. Hydrothermal pyrite was readily floatable (32 pct floated), indicating that its surface was positively charged and capable of electrostatically attracting the anionic collector. Adsorption of the collector rendered the surface hydrophobic and allowed the flotation of hydrothermal pyrite. Sedimentary pyrite was depressed, indicating that its surface was negatively charged and not able to interact with the anionic fluorosurfactant. The surface charge must be known in order to design coating agents that can be applied to pyritic material to limit oxidation. Because the charge on sedimentary pyrite surfaces is negative, a cationic species would provide the best coating. In the case of hydrothermal pyrite, an anionic species would be a better choice.

CONCLUSIONS

This study showed that pyrite of low-temperature origin (sedimentary pyrite) differs from pyrite of high-temperature origin (hydrothermal pyrite) in many basic properties:

1. The observed differences in oxidation rate between pyrites cannot be completely explained by differences in surface area;

2. The rate dependence of abiotic pyrite oxidation on oxygen content is considerably higher for sedimentary pyrite than for hydrothermal pyrite;

3. In evolved gas analysis, sedimentary pyrite evolves SO_2 at lower temperatures, indicating that it is more reactive than hydrothermal pyrite;

4. In plots of abiotic surface oxidation rate versus mean SO_2 evolution temperature, sedimentary pyrites and hydrothermal pyrites appear to form two discrete populations;

5. Surfaces of hydrothermal pyrite are positively charged (floats in flotation tests with anionic fluorsurfactant); surfaces of sedimentary pyrite are negatively charged (depressed in flotation tests).

Results of this study indicate that passivation of pyrite surfaces occurs rapidly once sufficient oxidation has taken place. This passivation is probably caused by the formation of a metal-deficient sulfide layer and the accumulation of oxidation products on pyrite surfaces. Passivation would probably not occur under field conditions where 1) there is sufficient moisture to dissolve and transport hygroscopic iron sulfates, and 2) there are bacteria that can oxidize metal-deficient sulfide layers.

A plot of surface oxidation rates measured by XPS versus SO_2 evolution temperatures from EGA can be described by two linear trends, one trend represented by five sedimentary pyrites, the second trend represented by three iron disulfides of predominantly hydrothermal origin. Based on these linear relationships, results from quick and simple EGA tests can now be used to calculate surface oxidation rates. For example, EGA results from 16 coal and 55 overburden samples indicate that the predominant surface oxidation rate for sedimentary pyrite is between 2.5- and 4.5 mg SO_4^{-2} g^{-1} FeS_2 hr^{-1}. These rates are abiotic rates based on available pyrite (pyrite at the surface) and cannot be directly applied to the field without considering surface area and bacterial catalysis. However, these results can be used to augment existing AMD predictive techniques by providing a qualitative ranking of iron disulfide reactivity. Their origin (sedimentary or hydrothermal) is critical to the type of behavior exhibited by iron disulfides. We know from previous work that sedimentary pyrites display a wide range of reactivities. The oxidation rates displayed by the three hydrothermal iron disulfides in the current study appear to be more consistent, perhaps reflecting a more highly ordered crystal structure. It is important to recognize that the fundamental properties of iron disulfides, particularly of sedimentary pyrite, can vary widely. Iron disulfides are similar in gross stoichiometry, but little else.

ACKNOWLEDGEMENTS

The authors would like to thank Dr. Sidney Pollack of DOE's Pittsburgh Energy Technology Center for the X-ray diffraction analysis of iron disulfide specimens. We would also like to thank Dr. Dick Souza, mineral curator of the Carnegie Museum for providing pyrite/marcasite and marcasite specimens for this study. Coal samples for EGA tests were provided by Dr. John Renton of West Virginia University. The authors acknowledge the efforts of John Kleinhenz, Doug Zeik, Debbie Kinzler, Bob Patton, and Trish Steffan who made this work possible.

LITERATURE CITED

Braley, S. A. 1960. The oxidation of pyritic conglomerates. Spec. Rept. to Coal Ind. Advisory Comm. to Ohio River Valley Water Sanit. Comm. Res. Proj. No. 370-6:32 p.

Buckley, A. N. and R. Woods. 1986. The surface oxidation of pyrite. Applied Surface Science 27:437-452. http://dx.doi.org/10.1016/0169-4332(87)90153-X

Buckley, A. N., R. Woods, and H. J. Wouterlood. 1987. The deposition of sulfur on pyrite and halcopyrite from sodium sulfide solutions. To be published in Proceedings of the Royal Australian Chemical Institute Eighth National Convention, Sydney, Australia.

Clark, C. S. 1965. The oxidation of coal mine pyrite. Ph.D. Thesis, the Johns Hopkins Univ. 90 p.

Esposito, M. C., S. Chander, and F. F. Aplan. 1987. Characterization of pyrite from coal sources. To be published In Process Mineralogy VII. A. H. Vassiliou(Ed.). TMS/AIME.

Guilinger, T. R., R. S. Schechter, and L. W. Lake. 1987. Kinetic study of pyrite oxidation in basic carbonate solutions. Ind. Eng. Chem. Res. 26:824-830. http://dx.doi.org/10.1021/ie00064a035

LaCount, R. B., R. R. Anderson, C. A. Helms, and S. Friedman. 1983. Construction and operation of a controlled-atmosphere programmed-temperature reaction apparatus. U.S. Dept. of Energy DOE/PETC/TR-83/5. 22 p. plus appendices.

Nicholson, R. V., R. W. Gillham, and E. J. Reardon. 1987. Pyrite oxidation in carbonate-buffered solution: 1 experimental kinetics. To be published in Geochimica et Cosmochimica Acta. https://doi.org/10.1016/0016-7037(88)90262-1

Pugh, C. E., L. R. Hossner, and J. B. Dixon. 1981. Pyrite and marcasite surface area as influenced by morphology and particle diameter. Soil Sci. Soc. Am. J. 45:979-982. http://dx.doi.org/10.2136/sssaj1981.03615995004500050033x

Pugh, C. E., L. R. Hossner, and J. B. Dixon. 1984. Oxidation rate of iron sulfides as affected by surface area, morphology, oxygen concentration, and autotrophic bacteria. Soil Science 137:309-314. http://dx.doi.org/10.1097/00010694-198405000-00003

Rogowski, A. S. and H. B. Pionke. 1984. Hydrology and water quality on stripmined lands. U.S. Environmental Protection Agency EPA-IAG-D5-E763. 183 p.